Experiments on PMMA models to predict the impact of corneal refractive surgery on corneal shape

Carlos Dorronsoro and Daniel Cano

Instituto de Optica "Daza de Valdés", Consejo Superior de Investigaciones Científicas, Serrano 121, 28006, Madrid, Spain
cdorronsoro@io.cfmac.csic.es

Jesús Merayo-Lloves

Instituto de Oftalmobiología Aplicada, Universidad de Valladolid, Edificio Ciencias de la Salud - Avda. Ramón y Cajal, 7 - 47005 Valladolid, Spain
merayo@ioba.med.uva.es

Susana Marcos

Instituto de Optica "Daza de Valdés", Consejo Superior de Investigaciones Científicas, Serrano 121, 28006, Madrid, Spain
susana@io.cfmac.csic.es

http://www.vision.io.csic.es

Abstract: Flat and spherical PMMA surfaces were ablated with a standard refractive surgery laser system. The ratio of profiles on flat to spherical PMMA surfaces was used to estimate experimentally the radial change in ablation efficiency for PMMA and cornea. Changes in ablation efficiency accounted for most of the asphericity increase found clinically, using the same laser system. This protocol is useful to obtain a correction factor for any ablation algorithm and laser system, and to estimate the contribution of biomechanics to the increase of corneal asphericity in myopic refractive surgery.

OCIS codes: (170.1020) Ablation of tissue; (170.3890) Medical optics instrumentation; (120.6650) Surface measurements, figure; (140.3390) Laser materials processing; (330.5370) Physiological optics; (330.4460) Ophthalmic optics; (220.1000) Aberration compensation

References and links

1. I. Pallikaris, M. Papatzanaki, E. Stathi, O. Frenschock, and A. Georgiadis, "Laser in situ keratomileusis," Lasers. Surg. Med. **10**, 463-468 (1990).
2. M. Mrochen, M. Kaemmerer, and T. Seiler. "Wavefront-guided Laser in situ Keratomileusis: Early results in three eyes," J. Refract. Surg. **16**, 116-121 (2000).
3. E. Moreno-Barriuso, J. Merayo-Lloves, S. Marcos, R. Navarro, L. Llorente and S. Barbero, "Ocular aberrations before and after myopic corneal refractive surgery: LASIK-induced changes measured with Laser Ray Tracing," Invest. Ophthalmol. Vis. Sci. **42**, 1396-1403 (2001).
4. S. Marcos, S. Barbero, L. Llorente, and J. Merayo-Lloves, "Optical response to LASIK for myopia from total and corneal aberrations," Invest. Ophthalmol. Vis. Sci. **42,** 3349-3356 (2001).
5. J. T. Holladay, D. R. Dudeja, and J. Chang, "Functional vision and corneal changes after laser in situ keratomileusis determined by contrast sensitivity, glare testing and corneal topography," J. Cataract. Refract. Surg., **25**(5), 663-669 (1999).
6. L. Llorente, S. Barbero, J. Merayo, and S. Marcos, "Changes in corneal and total aberrations induced by LASIK surgery for hyperopia," J. Refract. Surg., **20**, 203-216 (2004).
7. C. Munnerlyn, S. Koons, and J. Marshall, "Photorefractive keratectomy: a technique for laser refractive surgery," J. Cataract. Refract. Surg. **14**, 46-52 (1988).
8. D. Gatinel, T. Hoang-Xuan, and D. Azar, "Determination of corneal asphericity after myopia surgery with the excimer laser: a mathematical model," Invest. Ophthalmol. Vis. Sci. **42**, 1736-1742 (2001).

#69908 - $15.00 USD Received 17 April 2006; revised 12 June 2006; accepted 14 June 2006

9. J. Jiménez, R. Anera, and L. Jiménez del Barco, "Equation for corneal asphericity after corneal refractive surgery," J. Refract. Surg. **19**(1), 65-69 (2003).
10. S. Marcos, D. Cano, and S. Barbero, "The increase of corneal asphericity after standard myopic LASIK surgery is not inherent to the Munnerlyn algorithm," J. Refract. Surg. **19**, 592-596 (2003).
11. M. Mrochen, T. Seiler, "Influence of corneal curvature on calculation of ablation patterns used in photorefractive laser surgery," J. Refract. Surg. **17**, 584-587 (2001).
12. J. Jiménez, R. Anera, L. Jiménez del Barco, and E. Hita, "Effect on laser-ablation algorithms of reflection losses and nonnormal incidence on the anterior cornea," Appl. Phys. Lett. **81**(8), 1521-1523 (2002).
13. R. Anera, J. Jimenez, L. Jimenez del Barco, and E. Hita, "Changes in corneal asphericity after laser refractive surgery, including reflection losses and nonnormal incidence upon the anterior cornea," Opt. Lett. **28**, 417-419 (2003).
14. D. Cano, S. Barbero, and S. Marcos, "Comparison of real and computer-simulated outcomes of LASIK refractive surgery," J. Opt. Soc. Am. A. **21**, 926-936 (2004).
15. C. Roberts, and W. Dupps, "Corneal biomechanics and their role in corneal ablative procedures," in *Customized corneal ablation: The quest for super vision*, S. McRae, R. Krueger, and R. Applegate, eds. (Stack Publishing, 2001).
16. J. D. Gottsch, E. V. Rencs, J. L. Cambier, D. Hall, D. T. Azar and W. J. Stark, "Excimer laser calibration system," J. Refract. Surg. **12**, 401-411 (1996).
17. C. B. Odonnell, J. Kemner, and F. E. Odonnell, "Surface roughness in PMMA is linearly related to the amount of excimer laser ablation," J. Refract. Surg. **12**, 171-174 (1996).
18. A. M. Roszkowska, G. Korn, M. Lenzner, M. Kirsch, O. Kittelmann, R. Zatonski, P. Ferreri and G. Ferreri, "Experimental and clinical investigation of efficiency and ablation profiles of new solid-state deep-ultraviolet laser for vision correction," J. Cataract Refract. Surg. **30**, 2536-2542 (2004).
19. S. Marcos, "Aberrations and Visual Performance following standard laser vision correction," J. Refract. Surg. **17,** 596-601 (2001).
20. G. Pettit and M. Ediger, "Corneal-tissue absorption coefficients for 193- and 213-nm ultraviolet radiation," Appl. Opt. **35**, 3386-3391 (1996).
21. M. W. Berns, L. Chao, A. W. Giebel, L. H. Liaw, J. Andrews and B. VerSteeg, "Human corneal ablation threshold using the 193-nm ArF excimer laser," Invest. Ophthalmol. Vis. Sci., **40**, 826-830 (1999).
22. R. Srinivasan, "Ablation of polymers and biological tissue by ultraviolet lasers," Science, **234**, 559-565 (1986).
23. G. Pettit, "Practical issues of wavefront-guided refractive surgery," FIO/LS Conference Program 118, (2005).
24. J. R. Jimenez, R. G. Anera, J. A. Diaz, and F. Perez-Ocon, "Corneal asphericity after refractive surgery when the Munnerlyn formula is applied," J. Opt. Soc. Am. A **21**, 98-103 (2004).
25. B. T. Fisher and D. W. Hahn, "Measurement of small-signal absorption coefficient and absorption cross section of collagen for 193-nm excimer laser light and the role of collagen in tissue ablation," Appl. Opt. **43**, 5443-5451 (2004).
26. F. Manns, P. Milne, and J. M. Parel, "Ultraviolet corneal photoablation," J. Refract. Surg. **18**, 610-614 (2002).
27. S. Marcos, D. Cano, and C. Dorronsoro, "A method of preventing the induction of aberrations in laser refractive surgery systems," Patent WO 2005/122873 A1. (2005), http://v3.espacenet.com/textdoc?DB=EPODOC&IDX=WO2005122873.
28. D. Aizawa, K. Shimizu, M. Komatsu, M. Ito, M. Suzuki, K. Ohno and H. Uozato, "Clinical outcomes of wavefront-guided laser in situ keratomileusis: 6-month follow-up," J. Cataract Refract. Surg. **29**, 1507-1513 (2003).
29. A. I. Caster, J. L. Hoff, and R. Ruiz, "Conventional vs wavefront-guided LASIK using the LADARVision4000 excimer laser," J. Refract. Surg. **21**, 786-791 (2005).
30. C. Roberts "The cornea is not a piece of plastic," J. Refract. Surg. **16**, 407-413 (2000).

1. Introduction

Laser refractive surgery has become a popular procedure for the correction of refractive errors. In this technique, the patient's cornea is sculpted by UV laser ablation to change its shape aiming at correcting the refractive errors of the eye [1]. With the availability of flying spot lasers, which allow a better control of the laser energy delivery at each corneal position, there is an increased interest in refining the corneal ablation profiles. Customized ablation procedures aim at correcting not only defocus and astigmatism, but also high order aberrations [2]. The success of such type of corrections depends not only on a correct theoretical design of the algorithm but also on the proper transfer of the laser energy into the cornea, and a reliable knowledge of the corneal response.

#69908 - $15.00 USD Received 17 April 2006; revised 12 June 2006; accepted 14 June 2006

Standard laser refractive surgery, while successful at correcting defocus and astigmatism, has been shown to induce important amounts of spherical aberration in patients [3, 4]. Corneal asphericity increases (and spherical aberration increases towards more positive values) after refractive surgery for myopia [5], and corneal asphericity decreases (and spherical aberration shifts toward negative values) after refractive surgery for hyperopia [6]. This change in spherical aberration is highly correlated with correction. However, the causes for the change in corneal asphericity (and spherical aberration) are not fully understood.

The aim of this paper is to investigate the causes for the change in corneal asphericity (and spherical aberration) produced by refractive surgery. For this task we have developed an experimental model on PMMA surfaces, along with computer predictions and experimental data in patients obtained in previous studies in our laboratory, to assess the source of the increase of corneal asphericity after standard refractive surgery for myopia.

There are three possible reasons for the consistent increase in corneal asphericity after myopic LASIK: 1) the assumptions inherent to the theoretical ablation profile; 2) changes in laser efficiency from the apex to the periphery of the curved cornea; 3) the corneal biomechanical response and wound healing.

Several studies have estimated the changes in corneal asphericity expected from the theoretical application of the standard ablation pattern, using both the formula reported by Munnerlyn et al. [7], which assumes that both pre- and post-operative corneal shapes are spherical, or a parabolic approximation of the Munnerlyn formula. Numerical analysis performed by Gatinel et al. [8] demonstrates that the Munnerlyn pattern should not increase the asphericity of corneas with typical preoperative asphericities, in contrast to clinical findings. Jiménez et al. [9] carried out analytical calculations and found that the parabolic approximation of the Munnerlyn function should produce some increase in corneal asphericity after myopic corneal ablation.

In a recent study [10], we simulated post-operative corneal surfaces by subtracting the standard Munnerlyn ablation pattern and a parabolic approximation of the Munnerlyn pattern from real pre-operative corneas, and compared the estimated post-operative asphericity (Q) and spherical aberration with the real post-operative values. We found that while the actual surgical procedure increased asphericity from -0.14±0.14 to 1.1±1.3 on average, for treatments ranging between -2.0 to -11.5 D, corneal asphericities expected from the computer simulations with the standard Munnerlyn pattern did not increase (mean post-operative asphericity = -0.21±0.19). Simulations with the parabolic approximation of the Munnerlyn formula only increased slightly the corneal asphericities (mean post-operative asphericity = 0.3±0.4). These results indicate that the increase in corneal asphericity is not due to an inappropriate design of these ablation patterns, or the assumptions upon which these patterns are based.

Mrochen et al. [11] proposed that the increase of asphericity with the refractive surgery procedure is due to changes in the ablation efficiency as the laser spot moves from the center to the periphery of the cornea. As the angle of incidence α increases, both the reflected energy and the illuminated area increase and therefore, the ablation depth per pulse decreases. Ablation efficiency can be defined as the ratio of the amount of removed material when the angle of incidence is $\boldsymbol{\alpha}$ to the amount of removed material when the illumination is perpendicular to the corneal surface. Jiménez et al. [12, 13] estimated theoretically the corneal ablation efficiency -$K(\alpha)$ in this study- using Fresnel equations and taking corneal curvature into account. They provided an equation that relies on several assumptions regarding the laser properties and laser-tissue interactions. These assumptions include: 1) homogeneous laser beam intensity; 2) non-polarized light; and 3) Beer-Lambert's law, i.e. logarithmic dependence of the ablation depth on the absorbed energy density. In Jiménez's model, the resultant corneal shape after ablation depends not only on the laser fluence pattern but also on the corneal radius of curvature and on the tissue properties (ablation fluence threshold and refractive index) at 193nm.

In a previous study in our laboratory [14], we incorporated Jimenez´s expression for $K(\alpha)$ into our computer simulations of corneal refractive surgery on real pre-operative corneal

#69908 - $15.00 USD Received 17 April 2006; revised 12 June 2006; accepted 14 June 2006

topographies, in combination with both the exact Munnerlyn and the parabolic patterns. We found that changes in ablation efficiency as given by the theoretical expression of $K(\alpha)$ contribute to increase the asphericity of the ablated corneas. We found an average corneal post-operative asphericity of 0.3±0.4 when incorporating efficiency changes into the exact Munnerlyn equation, and 0.7±0.4 when incorporating efficiency changes into the parabolic approximation. While those values are still lower than those found in the real corneas, these results suggest that a parabolic ablation profile and, more importantly, ignoring the effects of corneal curvature on laser ablation efficiency are a major cause of the increased asphericity after myopic refractive surgery.

Some authors have investigated the impact of biomechanical response on refractive surgery outcomes. Roberts & Dupps [15] suggested that the breakage of lamellar structures during ablation could produce a redistribution of both corneal strain and intrastromal fluid. These authors proposed a corneal biomechanical model which explains the unintended hyperopic shift found in treated eyes. Differential epithelial growth and excessive wound healing after ablation have also been proposed to have an effect on final corneal shape.

The present study aims at testing experimentally the contributions of the ablation profile and laser efficiency to the change in corneal asphericity. Previous theoretical calculations and computer simulations involve several assumptions. First, they assume that the standard ablation pattern is based on the Munnerlyn formula, or the parabolic profile. However, these patterns are proprietary, and the theoretical profiles are not necessarily those programmed into the laser system. Second, corneal ablation efficiency has been estimated using the Jiménez et al.'s function $K(\alpha)$, but this equation relies on the mentioned assumptions. In this study we carried out experiments on PMMA (both flat and spherical surfaces) to identify the impact of the actual profile, and of laser efficiency changes across the curved surface. By comparison with predictions from computer simulations using Jiménez et al.'s function $K(\alpha)$, we will be able to assess experimentally the hypotheses involved in this formula.

Ablation of PMMA flat surfaces has been used before [16-18], with the aim of assessing the roughness created by the current ablation patterns. However none of these studied the changes in asphericity induced by the ablation patterns. In this paper, flat and spherical PMMA surfaces were ablated with a standard refractive surgery laser system. Spherical PMMA surfaces were made with similar radii of curvature than that of human corneas. Profilometric measurements of PMMA flat surfaces after ablation will test the actual ablation profile programmed into the laser system, and whether this is close to the theoretical Munnerlyn pattern. A comparison between the ablated spherical PMMA surfaces and identical ablations on flat surfaces will show the effects of laser efficiency changes across a curved PMMA surface. Once the difference in ablation rates between PMMA and corneal tissue are considered, as well as the differences in ablation threshold in PMMA and cornea, it is possible to estimate the effect of laser efficiency on post-operative corneal shapes. A direct comparison of real and model post-operative corneal shapes will give insight into the possible contribution of biomechanical and wound healing effects to the increase of corneal asphericity in myopic refractive surgery. The conclusions will be relevant both in the optimization of refractive surgery algorithms, and in the manufacture of phase plates and contact lenses by laser ablation.

2. Methods

2.1. Laser equipment

Laser ablation of polymethyl-methacrylate (PMMA) surfaces was carried out with a conventional flying-spot laser system used for corneal refractive surgery (Chiron Technolas 217-C equipped with the PlanoScan program; Bausch & Lomb Surgical). This system has an Argon Fluoride (ArF) excimer laser delivering laser pulses at 50Hz. The laser beam diameter is between 1 and 2 mm. The emission wavelength is 193nm and the radiance exposure is 120mJ/cm^2. The laser system is programmed to produce standard ablation patterns for correction of myopia, hyperopia and astigmatism. An identical equipment (operated by the

#69908 - $15.00 USD Received 17 April 2006; revised 12 June 2006; accepted 14 June 2006

same surgeon) had been used in the patients from previous studies [3, 4, 19] in our laboratory, used in this study as a reference.

2.2. PMMA model

Laser ablation was performed onto flat and spherical PMMA surfaces. PMMA was supplied by Horniplas (Vitoria-Gasteiz, Spain) in form of flat-faced pieces. To manufacture the spherical surfaces, the flat-pieces were firstly machined into 12-mm cylindrical rods. The spherical surface was grinded on one tip of the cylinder following standard procedures in a manual lathe. Polishing was performed with a polishing cloth damped with Orma Polish (Gerard Kluyskens Company, NYC, NY) with precise polishing tools on the same lathe. The intended radius of curvature was 8.00 mm, similar to that in human corneas. Surface curvature was initially checked in the workshop with an optical gauge and Newton rings.

Two types of PMMA were used for laser ablation: extruded and cast PMMA. Preliminary tests were performed on cast PMMA, although final experiments were done using extruded PMMA. We observed that ablation profiles on cast PMMA were less repetitive, with some of the samples showing central islands after ablation.

2.3. Laser ablation of flat and spherical PMMA surfaces

Ten refractive surgery ablations were performed on flat surfaces and seven on spherical surfaces. Tables 1 and 2 list the ablation parameters used for each procedure. Both flat and spherical surfaces were ablated with myopic corrections of 3, 6, 9 and 12 D (for the cornea) and with optical zone diameters from 5 to 7 mm. Transition zone was 2 mm in all cases. The laser system computer showed the ablation depth that the applied radiation produces on corneal tissue. The surgeon operating the laser system centered the ablation at the surface apex, taking the corneal reflex as a reference.

Table 1. Description of the ten refractive surgery ablations performed onto flat PMMA surfaces

Myopic correction (D)	**3**	**6**	**9**	**12**
Optical zone diameter (mm)	7	7	6,5	5
Central ablation depth (μm)	72	142	180	142
Number of ablations performed	3	3	2	2

Table 2. Description of the seven refractive surgery ablations performed onto spherical PMMA surfaces[a]

Myopic correction (D)	**3**	**3**	**6**	**6**	**9**	**12**	**12**
Optical zone diameter (mm)	6	7	6	7	7	6	7
Central ablation depth (μm)	52	72	103	142	208	202	273

[a]The mean radius of curvature of the PMMA spheres before ablation was 7.97 ± 0.03 mm.

2.4. Profilometry and topography measurements

Flat surfaces

The shapes of the ablated flat surfaces were measured with a contact profilometry system (Detek 3000) that provides the profile of a sample along a given direction. This apparatus uses a small probe tip that is placed on the sample and moves across in continuous contact with the surface. The tip movement, that outlines the surface profile, is registered in a computer as two vectors that represent the Cartesian coordinates of the profile. The operating range of this system is 0.2 mm (height) x 15 mm (across). For each ablated flat surface, the ablation profile was measured along two perpendicular directions passing through the center of the ablation.

#69908 - $15.00 USD Received 17 April 2006; revised 12 June 2006; accepted 14 June 2006

Spherical surfaces

The shapes of the spherical surfaces were measured by corneal topography before and after ablation, and by contact profilometry and confocal microscopy after ablation. The vertical range of the contact profilometry system used for the flat surfaces was not sufficient to measure the elevation differences in the spherical surfaces. Instead, a Talysurf contact profilometry system (Taylor-Hobson, Leicester, England) was used. This system has sufficient working range to measure the profile along the 12-mm diameter of the artificial cornea, and its resolution is higher than the roughness of the ablated surface (typically less than 1 μm). Additionally, the shape of ablated spherical surfaces were obtained using confocal microscopy profilometry (Plμ, Sensofar, Terrassa, Barcelona, Spain). This system works by imaging the surface at different planes of focus, and reconstructing the surface map from a set of images. Although the working range of this system is 17 mm (height) and 112 x 73 mm (across), only the central 4-mm region of the ablated model corneas could be tested with the maximum resolution.

Profilometry and microscopy measurements on ablated spherical surfaces were compared to corneal topography measurements on the same surfaces. For corneal topography we used a videokeratographer (Atlas Mastervue; Humphrey Instruments-Zeiss, San Leandro, CA) with Placido rings. The aim of this comparison was to assess the accuracy of corneal topography on ablated surfaces, using contact profilometry as a 'gold standard' and to assess the possibility of using conventional corneal topography in this study, which would allow more direct comparisons to clinical data on patients' corneas. Corneal topography measurements of pre-ablated spherical surfaces verified radii of curvatures of 7.97±0.03 mm. Corneal topography measurements on spherical surfaces immediately following ablation were not possible, since the scattering produced by the increased surface roughness prevented appropriate reflection of the Placido rings. With the aim of increasing the surface reflectance, ablated surfaces were cleaned with a paper tissue soaked by a slight-scratch-remover liquid before topographic measurements. This slight polishing process removes the small ablation debris fixed to the surface and also smoothes the roughness generated by the ablation. An additional purpose of the comparison of the profiles obtained from the videokeratography, and contact and confocal microscopy was to assess whether the polishing process altered the global shape of the surface. The average difference, given by the root mean square error (RMSE), between the elevations provided by Talysurf and videokeratographer was 0.724 μm over the central 8 mm. The confocal microscope, although provides accurate measurements of the surface, was rejected for this study, because it does not provide information on the peripheral non-ablated area (the reference surface), which is needed to calculate the absolute ablation depth at each point.

These data demonstrate that videokeratoscopy produces reliable data on post-ablated surfaces, at least within the ablation zone. For this reason, all data on pre- and post-ablated spherical surfaces presented in this study are based on videokeratoscopy.

2.5. Assessment of the ablation pattern generated by the laser system

Flat surfaces

The surface profiles on ablated flat surfaces should represent the actual ablation profiles produced by the laser. The support of the samples in the profilometry system was not necessarily perfectly parallel to the translation of the probe tip, causing some tilt in the measured profiles. The measured profiles were corrected numerically for this tilt, until the untreated areas appeared flat.

Spherical surfaces

The ablation patterns for spherical surfaces were obtained by subtracting the surface heights measured by videokeratography after ablation from the sphere with the pre-ablation curvature (as measured from videokeratography). As the reference axis for the videokeratographer (the

#69908 - $15.00 USD Received 17 April 2006; revised 12 June 2006; accepted 14 June 2006

line passing though the surface apex) may not coincide with the laser beam direction during ablation, the surface apex during topography measurements may not correspond with the ablation center. This may happen even if both ablation and measurement were well centered with respect to the surface circular limits. We wrote routines in Matlab (Mathworks, Nantick, MA) to rotate the measured corneal elevation profiles to bring the center (maximum depth) of the measured ablation to the apex, before subtraction. This results in a more precise (and symmetric) ablation pattern. In most cases, post-operative corneal elevation maps were repeated, tilting the cornea by the angle obtained from the programs, to align the ablation and measurement axes. This was achieved placing the base of the ablated model cornea on a tip-tilt table, and performing an iterative process until the estimated tilt and subsequent decentration were less than 0.2 deg and 0.05 mm respectively.

2.6. Ablation efficiency estimates

Ablation patterns on spherical surfaces are altered by variations in ablation efficiency due to changes in the angle of incidence of the laser beam as a function of surface location. In contrast, ablation efficiency is constant on flat surfaces, where laser incidence is always perpendicular. The ablation efficiency factor $K(\alpha)$ takes values between 0 and 1. From our measurements on PMMA, we will estimate $K(\alpha)$ by dividing the ablation profile measured on spherical surfaces by the ablation profile measured on flat surfaces, for the same conditions. This function describes the laser efficiency effects reducing the ablation depth at the periphery, and therefore the adjustment factor by which the laser ablation profile is multiplied to give the final ablation produced on curved surfaces. From a design point of view, $K(\alpha)$ represents the adjustment factor by which the intended profile should be divided to compensate for the changes in ablation efficiency on curved surfaces.

It should be noted that $K(\alpha)$ depends on the refractive index for the laser wavelength and the ablation threshold, and therefore if will be different for a material with different n and F_{th} . Following application of the Beer-Lambert law [12]:

$$K = 1 + a \cdot f(R) \tag{1}$$

where $a=1/ln(F_0/F_{th})$, with F_0 the laser fluence and F_{th} the ablation threshold, and $f(R)$ is a reflectivity function, depending on the surface location and material index of refraction, given by Fresnel equations. While the refractive index at 193 nm is similar in cornea and in PMMA (n_{cornea} = 1.52 [20]; n_{PMMA}=1.49), and therefore we will assume f (R) to be the same for both materials, the ablation threshold differs ($F_{th,\ cornea}$= 40 mJ/cm^2 [21]; $F_{th,\ PMMA}$= 80mJ/cm^2 [22]).

The ablation efficiency factor for the cornea K_{cornea} will be estimated from the experimental estimates of K_{PMMA} using the following expression:

$$K_{cornea}(\alpha) = 1 + (a_{cornea}/a_{PMMA}) \cdot (K_{PMMA}(\alpha) - 1) \tag{2}$$

2.7. Post-operative asphericities

In order to assess the asphericities produced by the actual ablation patterns when the effects of reflection losses and non-normal incidence are not present, we computed the post-operative asphericities produced on an spherical PMMA surface (radius = 8 mm) by the laser ablation profiles measured on flat surfaces. We used fitting routines written in Matlab, as described in a previous publication [14]. To consider efficiency changes, these surfaces were multiplied by the measured K_{PMMA} before calculating their asphericity. Central radii of curvature and asphericities were also directly computed from the surface elevation maps measured on PMMA ablated spheres.

Corneal ablation patterns were calculated by converting PMMA ablation depths into corneal ablation depths by using a PMMA-cornea ablation factor to account for the different ablation rates (material removed per pulse) in PMMA and in cornea. The simulated postoperative corneas were calculated by: 1) applying an overall depth offset to the ablation profile, to account for a different transition zone; 2) multiplying by the estimated K_{cornea}, to account for the effects of ablation efficiency changes; 3) subtracting the resulting corneal

#69908 - $15.00 USD Received 17 April 2006; revised 12 June 2006; accepted 14 June 2006

ablation patterns from the simulated preoperative corneas. In all cases, the preoperative cornea was simulated as a conic surface with a typical human corneal shape (Radius of curvature = 7.8 mm; asphericity = -0.2). Corneal asphericity was computed as described above.

3. Results

3.1. PMMA-cornea correction factor

The ablation rate is different on corneal tissue than extruded PMMA. A conversion factor was estimated, to account for the difference in the ablation depth per laser pulse between PMMA and cornea.

Figure 1(a) shows central ablation depths (for different refractive corrections) in both flat and spherical PMMA samples versus the nominal ablation depth displayed on the laser system. There is a good correlation between nominal central ablation depths in the cornea and those measured in PMMA, with a slope of 1.8 μm on cornea /1 μm on PMMA. Despite the good correlation, which was expected since the amount of material removed by each laser pulse must be the same in all samples, we considered that the ablation PMMA-cornea correction computed from the regression line may not sufficiently accurate for several reasons: 1) there appears to be an offset in the regression line, since it does not cross the origin; 2) we ignore the reliability of the information on nominal corneal ablation depth provided by the laser system; 3) the factor only relies on ablation depth on a single central location (which in the case of elevation maps of spherical surfaces from videokeratoscopy is obtained by interpolation).

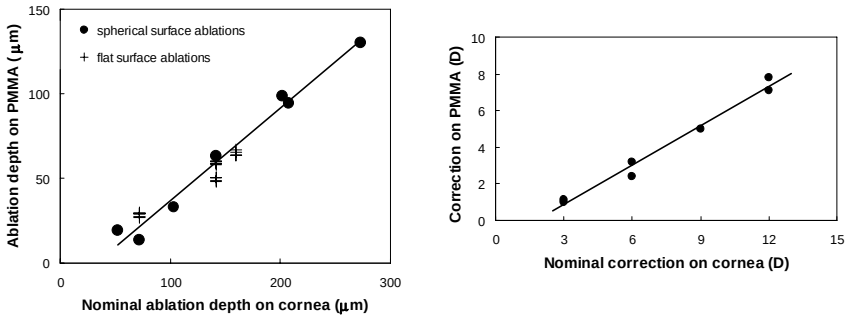

(A) (B)

Fig. 1. (a). Central ablation depths in flat –for two perpendicular meridians- (crosses) and spherical surfaces (solid circles). PMMA ablation depth was obtained from contact profilometry on flat surfaces, and videokeratography on spherical surfaces. Corneal ablation depth as provided by the laser system, for a given refraction correction and optical zone. The solid line represents the best-fitting line (slope = 0.55). (B) Refractive correction achieved on the spherical PMMA surfaces versus the intended correction on the cornea, as provided by the laser system. The solid line represents the best-fitting line (slope = 0.71).

Alternatively, we obtained the ablation rate factor between corneal tissue and PMMA as that producing the attempted corneal correction in simulated postoperative corneas. This was obtained after an iterative process in which, at each iteration of the factor, all ablations in flat PMMA were transformed into corneal ablations and their central radii compared with the intended value. With this approach we obtained a PMMA-cornea correction factor of 2.65. Ablation depths in PMMA have to be multiplied by this value to obtain corneal ablation depths.

Figure 1(b) shows a linear correlation between the nominal spherical correction on cornea and on PMMA. It should be noted that in Fig. 1(b) the refractive index of PMMA in the visible (n=1.49), rather than the corneal refractive index (n=1.377) was used to calculate the actual power change of PMMA ablated spheres.

#69908 - $15.00 USD Received 17 April 2006; revised 12 June 2006; accepted 14 June 2006

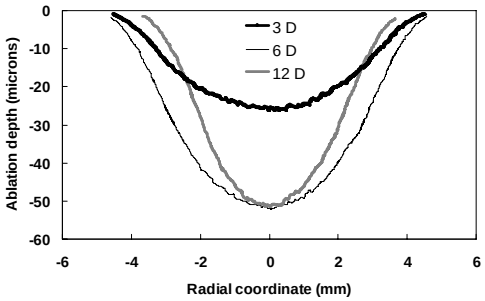

Fig. 2. Ablation profiles of three PMMA ablated flat surfaces for three nominal refractive myopic corrections (3, 6 and 12 D). Optical zone diameters were 7 mm for the 3-D and 6-D corrections and 5 mm for 12 D. These patterns were obtained by profilometry on ablated flat surfaces. These ablation patterns are not affected by ablation efficiency changes and represent the actual patterns for the cornea programmed into the laser system.

3.2. Ablation patterns from flat surfaces and from spherical surfaces

Figure 2 shows the profiles of three ablated PMMA flat surfaces, for three different corrections and optical zones. These ablation patterns are not affected by ablation efficiency changes and represent the actual patterns programmed into the laser system. It should be noted that the ablation depth depends both on the attempted correction and optical zone, and therefore two different corrections (i.e. 6 and 12 D) may result in similar central ablation depths.

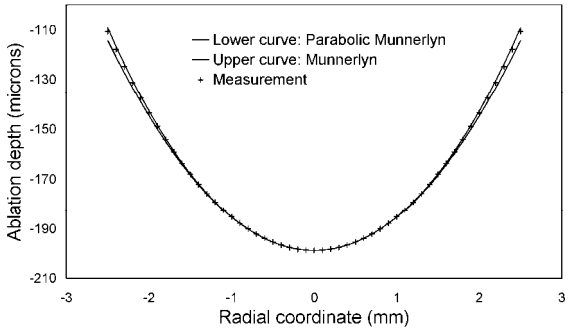

Fig. 3. Best fitting conic of the actual corneal ablation pattern -crosses- corresponding to the 12-D PMMA ablation pattern of Fig. 2, compared with the theoretical Munnerlyn and parabolic patterns -solid line- for the same correction and depth. The Munnerlyn pattern is calculated with the parameters of a typical preoperative cornea (radius 7.8 mm and asphericity -0.2).

Figure 3 shows one of the ablation profiles (12 D) of Fig. 2, after fitting to a polynomial curve, simulation of a different central ablation depth and multiplication by the PMMA-cornea correction factor, therefore representing ablation depths in cornea. For comparison, Fig. 3 also shows the theoretical Munnerlyn and the parabolic approximation of the Munnerlyn pattern, for the same correction. For this example, as in the majority of cases, the actual pattern programmed into the laser system is closer to the Munnerlyn pattern than to its parabolic approximation.

Figure 4 shows the shapes of two ablations measured on ablated PMMA spherical surfaces. This ablation patterns are affected by ablation efficiency changes across the curved surface.

#69908 - $15.00 USD Received 17 April 2006; revised 12 June 2006; accepted 14 June 2006

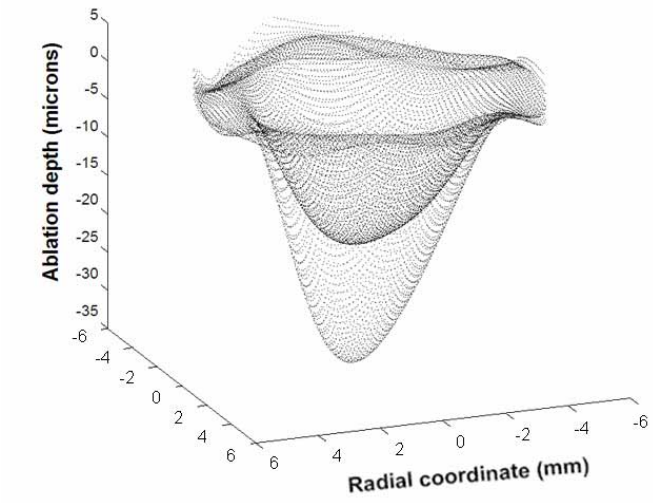

Fig. 4. Ablation profiles of two ablated PMMA spherical surfaces (3D:black dots, and 6D: gray dots), obtained by subtracting post-ablation elevation maps from the elevation maps of the spheres. This ablation patterns are affected by ablation efficiency changes across the curved surface. Outside the ablation the topographer has systematic errors, which are partially compensated after processing.

3.3. Experimental estimates of ablation efficiency

Figure 5 shows two ablation profiles on PMMA, one from a spherical surface (sections of all meridians superimposed), and another from a flat surface. Since both ablations have the same nominal correction (12 D), the energy profile delivered by the laser system is expected to be the same in both cases inside the central 5 mm (the smaller of the optical zones, indicated with vertical dashed lines in the plot). Therefore, the difference between both ablations (less penetration in the periphery of the ablated sphere) can only be attributed to laser efficiency losses.

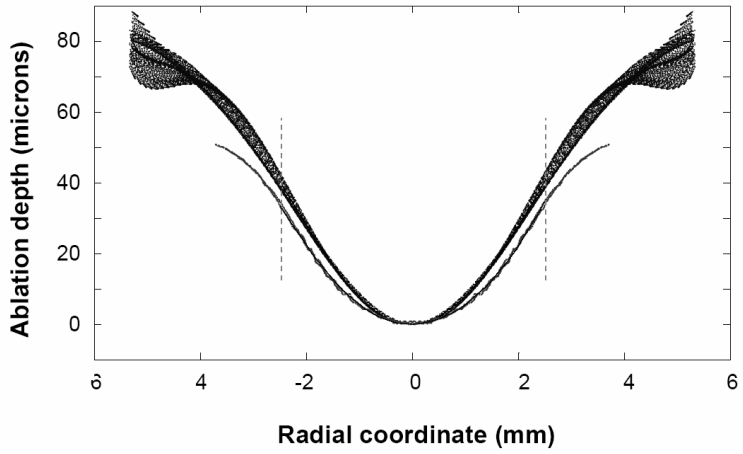

Fig. 5. Measurements of the ablation profile on PMMA from a spherical surface -upper curve- and a flat surface -lower curve- after myopic refractive surgery of 12 D. Although the optical zones are different, inside the central 5mm -vertical lines- the only expected difference among both measurements is due to laser efficiency losses. This produces a shallower ablation in the periphery of ablated spherical surfaces.

The profiles shown in Fig. 5 are highly symmetric, indicative of an accurate centration and alignment of the laser ablation, followed by an accurate measurement and processing. In many

#69908 - $15.00 USD Received 17 April 2006; revised 12 June 2006; accepted 14 June 2006

cases, the ablation profiles show slight defects or asymmetries, and for this reason the pair of ablation profiles shown in Fig. 5 were those used to estimate the ablation efficiency factor K. Figure 5 also shows the best fitting conics of these profiles, almost completely superimposed to the raw data. The ratio of these fitted curves were used directly to calculate the experimental ablation efficiency factor for PMMA (K_{PMMA}) shown in Fig. 6. The ablation efficiency factor for the cornea (K_{cornea}) is obtained from the experimental estimates of K_{PMMA} using Eq. (2). For comparison, Fig. 6 also shows theoretical estimates of K_{PMMA} and K_{cornea} using Jiménez et al's equations (that rely on the physical phenomena and the assumptions described in the introduction). Both the experimental and theoretical curves show a stronger ablation efficiency factor on PMMA than on the cornea. For both the cornea and PMMA, the theoretical factor seems to slightly underestimate the effect as compared to the experimental measurements. For example, at 2-mm from the corneal apex, laser efficiency decreases by 0.89 for PMMA from experimental measurements (0.92 theoretically) and 0.96 for the cornea (0.97 theoretically). The ablation rate of the material (or the PMMA-cornea correction factor) modulates the impact of the ablation efficiency factor $K(\alpha)$ on the final shape. For this reason, although K_{PMMA} is stronger than K_{cornea}, efficiency effects turn out to be more important in cornea that in PMMA.

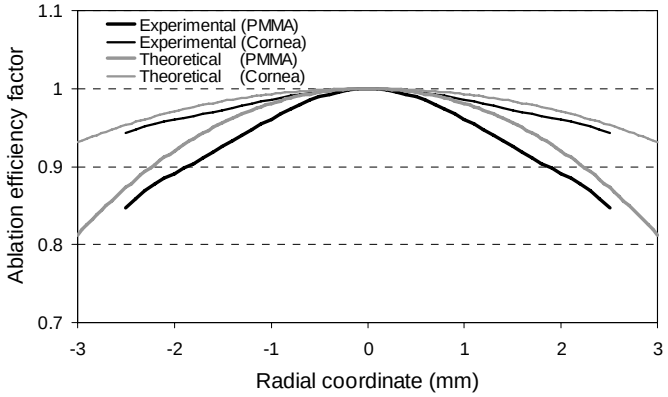

Fig. 6. Ablation efficiency factors obtained experimentally (black) for PMMA and cornea, compared with theoretical predictions using Jiménez et al's equations [12] for PMMA and cornea respectively. Data for PMMA are represented in thick lines and for the cornea in thin lines.

3.4. Post - operative asphericities on PMMA

Figure 7 shows postoperative asphericities estimated directly from the elevation maps of PMMA spherical surfaces (open circles), for different spherical corrections (the values indicate nominal corrections on the cornea, see Fig. 2(b) for the equivalent corrections on PMMA). We found a systematic increase of asphericity in all the surfaces tested, the larger the correction the larger the increase. The graph also plots the predicted asphericities using the experimental ablation efficiency factor found in this study (solid diamonds) and the theoretical efficiency factor (crosses) proposed by Jimenez et al. [12], calculated with the values corresponding to PMMA material. The predicted ablation pattern is the result of direct subtraction of the experimental ablation pattern measured on flat surfaces multiplied by the efficiency factor considered from a spherical surface of 8 mm-radius. The asphericities without considering efficiency effects (ablations on flat surfaces computationally applied to the spherical surfaces) are also shown (open diamonds). Without efficiency effects, the measured ablations have asphericities close to zero (-0.03±0.1, mean and standard deviation), and no change with correction. We found experimentally a significant increase of asphericity that can be entirely attributed to reflection losses and non-normal incidence. The mean asphericity of ablated PMMA spheres was 0.89 ±0.76.

#69908 - $15.00 USD Received 17 April 2006; revised 12 June 2006; accepted 14 June 2006

The asphericity predictions using the ablation profile from flat surfaces and the experimental efficiency factor agree well (0.93±0.37) with those obtained directly from experimental elevation maps on ablated PMMA spheres. For the 12-D sphere used in the calculation of the experimental efficiency factor, the coincidence is perfect, as expected. The theoretical efficiency factor predicts a mean increase in asphericity of 0.33±0.18, that is, 37% of the increase found experimentally.

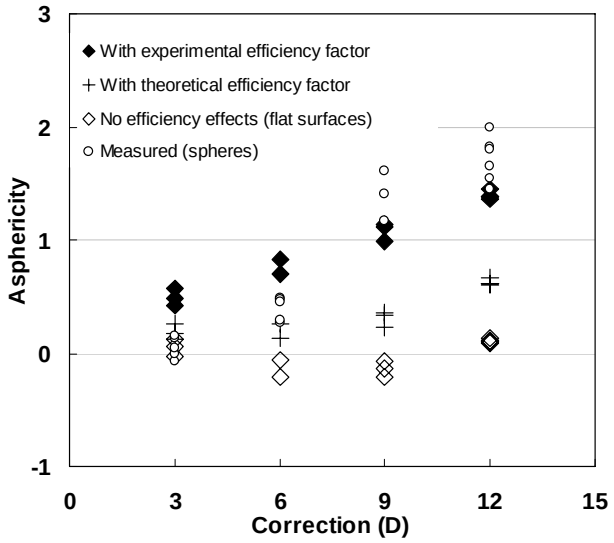

Fig. 7. Postoperative corneal asphericities of ablated PMMA surfaces as a function of nominal (on cornea) refractive correction, as measured directly on ablated spherical surfaces -open circles-. The figure also shows the predicted asphericity after direct subtraction of the experimental pattern measured on flat surfaces (non affected by efficiency factor) -open diamonds- as well as subtraction of this pattern multiplied by the experimental -solid diamonds- and theoretical -crosses- efficiency factors for PMMA. Pre-operative spherical surfaces had radii of curvature of 8-mm.

3.5. Post - operative asphericities on cornea

Our predictions of corneal asphericity using the experimental ablation pattern (actual profile programmed in the laser system) and our experimental estimates of K_{cornea} can be compared directly to data on real patients.

Figure 8 shows postoperative clinical asphericities compared with predicted corneal asphericities as a function of spherical correction. Clinical asphericities (open triangles) were measured in patients treated with standard refractive surgery from a previous study in our laboratory [4], with an identical laser operated by the same surgeon. Predicted asphericities were calculated from experimental data, for a typical preoperative cornea of radius 7.8 and asphericity -0.2. To simulate the postoperative cornea, the ablation measured in flat surfaces is multiplied by the PMMA-cornea correction factor and by the ablation efficiency factor K_{cornea}, and then directly subtracted from the preoperative cornea. Predictions without considering efficiency effects (open diamonds) show practically no change of corneal asphericity with ablation (-0.43±0.40). Predictions using Jimenez's theoretical K_{cornea} –thick gray line in Fig. 6– (crosses) show a slight increase of asphericity with attempted correction (0.03±0.49). Predictions using the experimental K_{cornea} from the current study –thick black line in Fig. 6– (solid diamonds) show significantly higher corneal asphericities (0.78±0.70). It should be noted that throughout the study we have used a rather conservative value for corneal ablation threshold (Fth=40 mJ/cm^2). Figure 8 also shows predictions with K_{cornea} estimated with a recently reported [23] higher value –Fth=60 mJ/cm^2– (gray diamonds) which approaches even

#69908 - $15.00 USD Received 17 April 2006; revised 12 June 2006; accepted 14 June 2006

more (1.39±0.92) the asphericity values found clinically (open triangles) (1.97±2.00 considering the same set of corrections). This change in the corneal ablation threshold affects only slightly the predictions of the theoretical factor (0.29±0.53) (not shown).

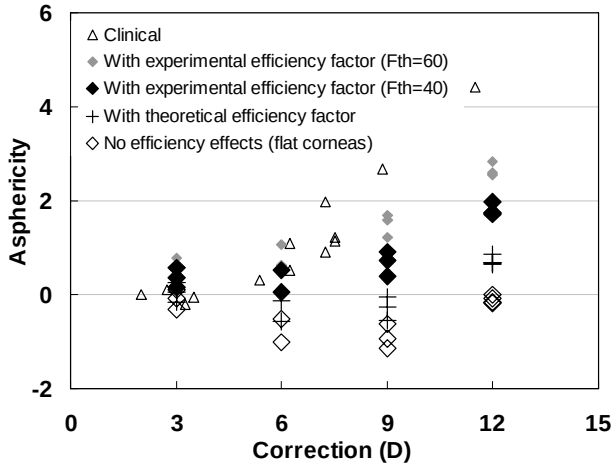

Fig. 8. Asphericities of simulated postoperative corneas (central radii 7.8 mm, asphericity -0.2) as a function of nominal correction, in comparison with clinical data (triangles) on real patients operated with the same laser system. Predictions include asphericities obtained from post-operative corneas after subtracting the corneal ablation pattern obtained from flat PMMA, i.e. with no efficiency effects (open diamonds), as well as this pattern multiplied by the experimental (solid diamonds) and the theoretical efficiency factor (crosses). Two different experimental efficiency factors (considering two different corneal ablation thresholds) were used, for $F_{th,\ cornea}$=40 (black) and with $F_{th,\ cornea}$=60 (gray).

In summary, the predicted corneal asphericities from the experimental efficiency factor are higher than those obtained with the theoretical factor, although for the highest corrections they are still lower than the clinical data on patients.

4. Discussion

4.1. Ablation pattern programmed into the laser

The comparison of the theoretical ablation patterns with the experimental ablation pattern (all shown in Fig. 3) suggests that the actual pattern programmed into the laser is close to the theoretical equations (Munnerlyn and parabolic). In addition, corneal asphericities induced purely by the experimental ablation pattern (see open diamonds in Fig. 8), without taking into account ablation efficiency changes and corneal biomechanics are close to those induced by the Munnerlyn pattern and show almost no change with correction, as reported before from analytical [8,24] and computational simulations [10, 14] of the Munnerlyn algorithm. Those asphericity predictions are far from the post-operative asphericities in real patients, indicating that the ablation profile *per se* is not the cause for the increased asphericity found clinically.

4.2. Experimental estimates of the ablation efficiency correction factor

As opposed to ablation patterns obtained from ablated flat PMMA surfaces, ablation patterns calculated from ablated spherical PMMA surfaces are affected by changes in ablation efficiency, i.e. the ablation depth per laser pulse decreases as the spot moves from the apex to the periphery, due to variations in the angle of incidence of the laser radiation. Measurements on both flat and spherical PMMA surfaces have allowed us to obtain a direct estimate of the ablation efficiency factor on PMMA, and a prediction of the ablation efficiency factor for the cornea based on those measurements. Previous estimates of the ablation efficiency factor had been obtained mathematically [12, 13], using approximations as a truncated polynomial series expansion, and assuming only reflection losses using Fresnel equations and non-polarized

#69908 - $15.00 USD Received 17 April 2006; revised 12 June 2006; accepted 14 June 2006

light, along with nominal values for laser fluence and corneal refractive index and ablation thresholds. However, there are other effects that potentially affect the changes in laser efficiency. These include spot shape, beam divergence changes from the center to the periphery, beam scanning effects, polarization, defocus, etc. Unlike the theoretical factor, the experimental ablation efficiency factor K_{PMMA} −and K_{cornea} estimated from K_{PMMA}− include these effects. While K_{PMMA} is a direct measurement of the ablation efficiency changes on PMMA and does not rely on any assumption, the estimates of the experimental K_{cornea} from the experimental K_{PMMA} rely on three assumptions: 1) that the Beer-Lambert's law applies to the cornea as well as on PMMA. 2) that the reflectivity factor *f(R)* is similar in PMMA and corneal tissue, which is true provided that the index of refraction at the laser wavelength is the same on cornea and PMMA and 3) that the laser fluence and the ablation thresholds for PMMA and corneal tissue are known. The fact that the Beer-Lambert´s law appropriately describes photoablation of corneal tissue is fairly well established [20, 25]. We have also tested assumption 2 by computing the difference in the reflectivity factor when changing the index of refraction by 1.52 instead of 1.49 and found no appreciable change. For PMMA, an ablation threshold of 80 mJ/cm^2 seems to be an accepted value. For the cornea however, while many studies use 40 mJ/cm^2 [21], some authors have recently reported [23] 60 mJ/cm^2. The ablation efficiency factor that we present represents therefore a conservative estimate. We repeated the computations using a corneal ablation threshold of 60 instead of 40 mJ/cm^2 and found predicted corneal asphericities closer to the clinical estimates, as shown in Fig. 8 (gray solid diamonds). Tissue hydration, that causes changes in reflectivity and absorption, among other effects, during corneal ablation [26], could also modify the laser ablation rate in corneas, and the cornea/PMMA factor.

Our experimental ablation efficiency factor K_{cornea}, although slightly stronger, agrees well with the theoretical K_{cornea} from Jimenez et al.'s (Fig. 6). However, the impact of this slight difference is important, and the predicted corneal asphericities using the experimental K_{cornea} are much closer to the clinical findings (Fig. 8). A similar effect was found on PMMA (Fig. 7).

The calibration protocols that we describe here can be generalized to any laser system and any material (with a refractive index similar to the cornea at the ablation wavelength), even if the numerous assumptions and simplifications of the theoretical model do not hold. This systematic calibration [27] will potentially be more effective than ablation efficiency factors empirically obtained by adjusting recursively the algorithm, which require prior treatments on real patients at different stages of the ablation algorithm refinement.

4.3. Impact of correction factors on post-operative corneal shape and aberrations

The experiments described here aim at explaining the increased asphericity found in eyes after standard LASIK for myopia, and at obtaining experimentally an ablation efficiency correction factor which corrects for the effect of laser efficiency changes across the cornea. As we tested experimentally, the laser system was programmed using a pattern close to the standard Munnerlyn algorithm with no further correction factor. Current generations of laser systems incorporate more sophisticated algorithms, aiming at canceling not only pre-operative sphere and cylinder but also high order aberrations. The application of ablation efficiency correction factors, as derived here, is essential to avoid induction of spherical aberration by surgery (associated to the increased asphericity described here) which would override the benefits of the individual high order aberration correction. In fact, reports on the outcomes of wavefront guided refractive surgery still show an increase of spherical aberration [28, 29]. As an example, Fig. 9 shows wave aberration maps (for 3rd and higher order aberrations) for a patient before surgery (-5 D pre-operative spherical error), and the wave aberration after simulation of wavefront guided refractive surgery, not including the ablation efficiency correction factor, and including it (not considering biomechanical factors). Correction of ablation efficiency avoids induction of spherical aberration.

#69908 - $15.00 USD Received 17 April 2006; revised 12 June 2006; accepted 14 June 2006

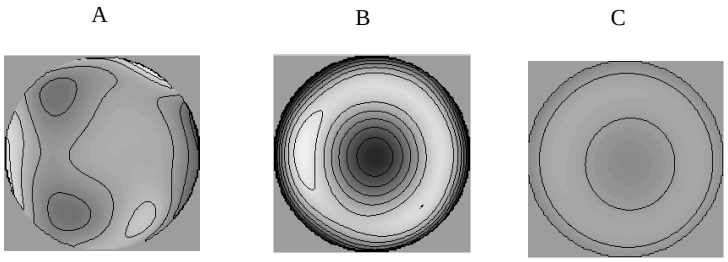

Fig. 9. Wave aberration maps (for 3rd and higher order aberrations) for a patient before LASIK (-5 D pre-operative spherical error, contour lines stand for 1 micron aberration steps) (A), and the wave aberration after simulation of wavefront guided refractive surgery, not including the ablation efficiency correction factor (B), and including it (C). Biomechanical factors are not considered. Correction of ablation efficiency avoids induction of spherical aberration.

4.4. The role of corneal biomechanics

The fact that the actual ablation patterns, when not affected by changes in ablation efficiency, do not produce major changes in corneal asphericity (and therefore do not induce the dramatic increase in spherical aberration found clinically) indicates that improvement in refractive surgery outcomes should rely not so much on a refinement of the theoretical design of the ablation patterns but their correction for both changes in ablation efficiency and biomechanical effects. Those effects need to be also taken into account when designing customized ablation algorithms.

Our experiments on PMMA spherical surfaces show that a non-biological material shows an important increase of asphericity after ablation, highly correlated with the amount of correction, indicating that a purely physical effects may have been previously underestimated [30]. We have demonstrated experimentally that changes in ablation efficiency across the cornea account for most of the asphericity increase found clinically. Models in PMMA are therefore useful to obtain the correction factor to be applied in the algorithm to compensate for changes in ablation efficiency across the cornea, and to validate the assumptions implicit in theoretically derived correction factors. However, the increase of corneal asphericity found clinically is not fully explained by results obtained in a PMMA corneal model, particularly for high corrections, leaving some room to biomechanical and wound healing factors.

5. Conclusions

A factor accounting for laser ablation efficiency changes from the center to periphery of the cornea has been obtained experimentally from laser ablation of flat and spherical polymethyl-methacrilate surfaces using a surgical excimer laser. Measurements after laser ablation with different amounts of myopic corrections show an important increase of corneal asphericity, caused by laser efficiency changes and not by the ablation algorithm, and explain most of the increase in asphericity found clinically (in patients operated with an identical laser system). This factor can be used by the laser manufacturers to compensate any laser ablation algorithm from induction of spherical aberration.

Acknowledgments

Andrés García Tante (CIDA, Madrid) manufactured the artificial corneas, Antonio Baeza (Indra, Aranjuez, Spain) and Fernando Sánchez (CIDA) performed contact profilometry and José Sáez Landete (Universidad Complutense de Madrid) confocal profilometry. Charlie Campbell provided helpful suggestions. Ablations on PMMA were performed at Centro Oftalmologico de Madrid. Support from Unidad Asociada IO-CSIC/IOBA-Universidad de Valladolid is also acknowledged. This research was funded by Grants BFM2002-02638 and FIS2005-04382 (Ministerio de Educación y Ciencia, Spain) and GR/SAL/0387/2004 (Consejería de Educacion Comunidad Autónoma de Madrid) to Susana Marcos. Daniel Cano was funded by a predoctoral fellowship from Comunidad Autónoma de Madrid.

#69908 - $15.00 USD Received 17 April 2006; revised 12 June 2006; accepted 14 June 2006